minerals

MDPI

Article

Scale Effect of Filling on Overburden Migration in Local Filling Stope of Longwall Face in Steeply Dipping Coal Seam

Shidong Wang [1,2], Wenyu Lv [2,3,4,*], Wenzhong Zhang [1,2], Juan Fan [1,2], Ankun Luo [1,2], Kaipeng Zhu [1,2] and Kai Guo [3]

[1] Hydrogeology Research Institute, Xi'an Research Institute of China Coal Technology and Engineering Group Corp, Xi'an 710054, China; wangshidong@cctegxian.com (S.W.); zhangwenzhong@cctegxian.com (W.Z.); fanjuan@cctegxian.com (J.F.); luoankun@cctegxian.com (A.L.); zhukaipeng@cctegxian.com (K.Z.)
[2] Shaanxi Province Key Laboratory of Coal Mine Water Disaster Prevention and Control Technology, Xi'an 710077, China
[3] School of Energy Engineering, Xi'an University of Science and Technology, Xi'an 710054, China; 20103077017@stu.xust.edu.cn
[4] Henan Key Laboratory for Green and Efficient Mining & Comprehensive Utilization of Mineral Resources, Henan Polytechnic University, Jiaozuo 454000, China
* Correspondence: lvwenyu2816@126.com

Abstract: The gangue filling mining method is used to reduce the occurrence of dynamic disasters on the roof of a steeply dipping coal seam (SDCS) effectively and improve the stability of the overburden structure. To comprehensively study the movement law of the overburden under different filling quantities, the 3221 working face of the Lvshuidong coal mine was taken as the research site. The vertical displacement, vertical stress, and plastic zone of the overburden under different filling quantities were analyzed by using FLAC3D numerical simulation and physical similarity simulations. The results show that the maximum stress in the stress concentration zone decreased with the increase of filling size. The vertical stress range of the overburden and floor in the filling zone increased significantly. The affected zones of the vertical displacement of the roof and floor and the vertical displacement of the overburden were reduced to varying degrees. The overall plastic zone was shrinking. The movement of overburden was well-controlled as the proportion of the fillings increased. The results of this study can provide an important reference for the stability control of the roof of SDCS filling mining.

Keywords: steeply dipping coal seam; numerical simulation; overburden migration; filling; scale effect

Citation: Wang, S.; Lv, W.; Zhang, W.; Fan, J.; Luo, A.; Zhu, K.; Guo, K. Scale Effect of Filling on Overburden Migration in Local Filling Stope of Longwall Face in Steeply Dipping Coal Seam. *Minerals* **2022**, *12*, 319. https://doi.org/10.3390/min12030319

Academic Editor: Abbas Taheri

Received: 10 January 2022
Accepted: 1 March 2022
Published: 4 March 2022

1. Introduction

The steeply dipping coal seam (SDCS) refers to the coal seams with a dip angle from 35° to 55°, which are recognized as difficult coal seams at home and abroad. Its reserves account for 10–20% of China's total coal resources, and more than 50% are scarce coal [1,2]. Therefore, it is urgent to ensure the safe and efficient mining of SDCS. In the process of SCDS longwall caving mining, the deformation, failure, and migration characteristics of roof strata in the middle and upper inclined zone of the working face are active [3–5]. In this range, the contact load characteristics between the roof and the support are complex, and the working load of the support system becomes smaller and uneven, which aggravates the sliding, falling, squeezing, and occlusion of the supports, and can easily cause safety accidents [6–8]. The gangue filling coal mining technology can control rock movement and surface subsidence, improve the recovery rate of "three under" pressed coal resources, solve the problem of gangue discharge, and effectively suppress the dynamic phenomenon of coal seam and roof and floor, which is conducive to improving the stability of surrounding rock [9–14]. This technology is gradually becoming one of the core technologies for green mining of coal resources in China. It is a major transformation to realize the ecological safety production environment in mining zones from passive governance to active prevention and control [15–18].

Many scholars have studied the behavior law of ground pressure, roof and overburden deformation, failure and migration law, support–surrounding rock interaction and stability control, and surface subsidence law of SDCS mining. Xie P.S. et al. [19] showed that the interaction between an inclined masonry structure and support can be divided into positive pressure and inclined extrusion, and reverse inclined and backward push strike extrusion based on many field practices, experimental studies, and theoretical analysis. The mechanical model of support–roof contact is established based on the basic dynamics and "R-S-F" dynamic control theory. Yao Q. et al. [20] studied the instability mechanism of the steeply inclined segmented filling column and proposed that the spacing of the filling column is positively related to the support reaction force of the filling column and the maximum bending moment of the roof. Guo J.Z. et al. [21] used numerical simulation software FLAC3D to establish the corresponding analysis model based on current research results and engineering practices of SDCS and simulated the characteristics of roof collapse and surrounding rock stress distribution in coal seam mining. Starting from the dip direction and length of the working face, the stress distribution law, deformation characteristics, and mining influence range of the surrounding rock at the upper and lower ends of the working face were emphatically analyzed. Xiao J.P. et al. [22] explored the evolution characteristics of overburden deformation, instability, and fracture in SDCS. The deformation and failure law of the overburden in SDCS is analyzed. The forms of roof failure and instability in SDCS under direct overburden thick sandstone and no hard rock stratum are discussed. Wang H.W. et al. [23] analyzed the influence of SDCS mining thickness on coal wall stability. The stress distribution of the coal wall in the working face is asymmetric, and the vertical displacement of the coal wall is much greater than the horizontal displacement. Dudek M. et al. [24] used the finite element model (FEM) to simulate the groundwater-induced surface deformation during SDCS extraction. Practice shows that the numerical model can better predict the surface deformation during SDCS mining. Ross C. et al. [25] creatively applied design criteria, including alternating mining depths and starting to mine thick seams towards the bottom of the seam, improving the recovery rate and stability during SDCS and thick coal seam mining.

The current research mainly focuses on the ground pressure behavior, deformation, failure, and migration laws of the roof and overburden under the unfilled condition of SDCS. Due to the complex mining conditions of SDCS, many basic theories for filling mining needed to be further studied. For example, the state of filling is the main controlling factor which affects the control of the roof stability in filling mining. At present, no systematic and in-depth research on the scale effect of the overburden migration in the local filling of steeply dipping coal seams is carried out, and the mechanism is still unclear. This paper takes the filling quantities as the main index. The physical similarity simulation and numerical simulation software FLAC3D are used to study the migration law of overburden in SDCS mining under different filling conditions, revealing the scale effect of the filling and providing a reference for the roof stability control of SDCS.

2. Project Overview

The fully mechanized mining face 3221 of Lvshuidong coal mine in Sichuan is located in the upper part of the 322 mining zone on the west wing of the Daluowan anticline +350 m horizontal in Lvshuidong coal mine. The upper working face 5614 has been mined, and the southern 3222 has not been excavated. The surface is dominated by mountains, high in the east and low in the west. The surface undulation is small, and the topsoil layer is mostly thin yellow mud. The surface elevation of the working face is from +830 to +930 m, the thickness of the coal seam is from 3.07 to 3.56 m, and the average thickness is 3.2 m. The dip of the coal seam is ~302°, the dip angle is 36°~42°, and the average dip angle is 40°. The coal seam is a semi-dark and semi-bright coking coal with a simple structure, with a vitreous luster and a hardness coefficient of ~1.5. The pseudo roof of the coal seam is gray clay mudstone with an average thickness of 0.15 m, which contains plant roots and leaves fossils and has strong water absorption. The upper part of the immediate roof is dark gray mudstone, and the lower

part is gray calcareous mudstone, with an average thickness of 8.60 m. The upper part of the main roof is dark gray mudstone, the middle part is argillaceous limestone, and the lower part is gray-black siliceous thin layer limestone, with an average thickness of 7.20 m. The direct floor is gray limestone and gray-white fine sandstone, with an average thickness of 0.70 m. The upper part of the main floor is medium-thick fine sandstone, the middle part is medium sandstone, and the lower part is gray-white bauxite, rich in pyrite nodules, with an average thickness of 6.60 m. The roof and floor of the working face in the whole zone are complete. The local filling mining method was adopted, as shown in Figure 1. The mechanical parameters of coal and rock are shown in Table 1.

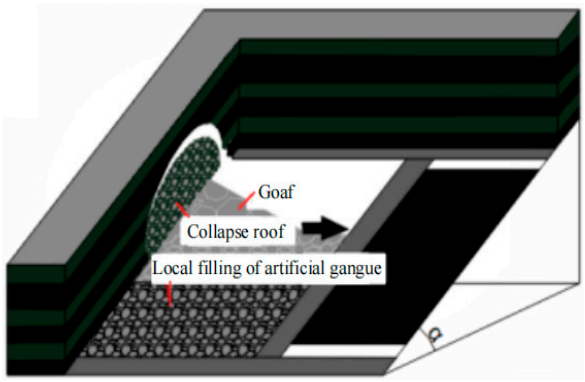

Figure 1. Local filling mining method with artificial gangue. As shown in this figure, the grey blocks represent goaf, the green and black blocks represent collapse roof, and the gray-black blocks represent the local filling of artificial gangue.

Table 1. Mechanical parameters of coal and rock.

Rock Type	Rock Name	Bulk Density	Volume Modulus	Shear Modulus	Poisson's Ratio	Compressive Strength	Cohesion (MPa)	Internal Friction Angle (°)
		(kg/m^3)	(GPa)	(GPa)		(MPa)		
Main roof	Marl	2950	5.0	3.7	0.23	34	4.9	36.9
Immediate roof	Sandy Mudstone	2510	4.2	3.0	0.32	20	2.0	31.1
Coal seam	Coal	1440	1.5	1	0.30	6	1.0	27.6
Immediate floor	Mudstone	2510	4.2	3.0	0.34	20	2.0	28.3
Main floor	Sandstone	2369	2.8	1.8	0.21	21	3.4	29

3. Model and Analysis of Numerical Calculation

Taking the engineering geological conditions of the working face 3221 of Lvshuidong coal mine as the research background, the basic numerical calculation mechanical model shown as Figure 2 was established according to the geological simulation of the working face. The length × wide × height of this model was 300 m × 240 m × 300 m. The Mohr–Coulomb plastic model built in FLAC3D was adopted as the constitutive model, and the large strain deformation mode was adopted throughout the operation process [26–28]. In order to be closer to the engineering practice, the physical and mechanical parameters of the coal seam and main rock layers were obtained according to the geological data and laboratory rock mechanics experiment results. The Mohr–Coulomb yield criterion was used to judge the failure of rock as follows:

$$f_s = \sigma_1 - \sigma_3 \frac{1+\sin\varphi}{1-\sin\varphi} - 2c\sqrt{\frac{1+\sin\varphi}{1-\sin\varphi}} \quad (1)$$

where σ_1 and σ_3 are the maximum and minimum principal stresses, respectively, and c and φ are the bonding force and friction angle, respectively. When $f_s > 0$, the material will

undergo shear failure. According to the tensile strength criterion, it can be judged whether the rock mass has tensile failure.

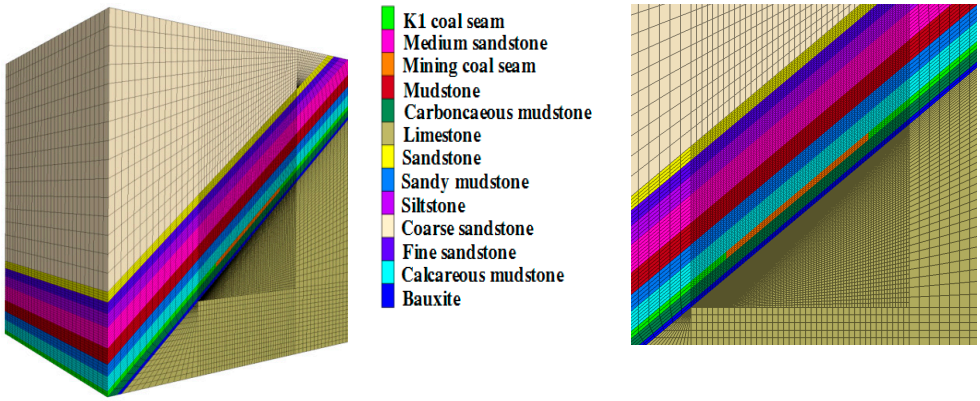

(**a**) (**b**)

Figure 2. The numerical simulation benchmark model. Blocks of different colors represent different layers as shown in the legend of (**a**). (**a**) 3D drawing of model; (**b**) Front view of the model.

The mining height of the coal seam was 3.2 m, the length of the working face was 105 m, and the inclination angle was 40°. The whole model consisted of 936,870 elements, including 965,705 nodes. The simulated filling ratios were no filling, 1/5, 1/3, 1/2, and 2/3, respectively.

The principle of changing a single variable was adopted in simulating mining under various operating conditions. Each operating condition model adopted the longwall working face mining method to simulate filling mining. The boundary conditions of the model were set as follows: vertical displacement was restricted at the bottom of the model, and horizontal displacement was restricted at the front, rear, left, and right sides of the model. Fix command was used to set boundary conditions [29–31]. In the x-axis direction, the x-direction velocity of all nodes on the plane of $x = 0$ and $x = 300$ was fixed. In the y-axis direction, the y-direction velocity of all nodes on the plane of $y = 0$ and $y = 300$ was fixed. In the z-axis direction, the z-direction velocity of all nodes on the plane of $z = 0$ was fixed. The main variable in the FLAC program was the node velocity, so the boundary conditions were also set according to the concept of velocity. The initial velocity of the node was zero as the model was not performing any operations. At this time, if the velocity of the node was fixed, it was equivalent to applying a fixed displacement boundary condition. In order to make the simulation results more realistic, a uniform compensation load of 8 MPa was applied downward to the upper surface of the model, and the in situ stress balance was carried out before simulating mining. In the process of model establishment, the influence of the boundary effect on the model calculation was considered. Therefore, the coal pillars with a certain width were left at the front, rear, left, and right of the working face to reduce the boundary effect.

3.1. Vertical Stress Distribution Characteristics of Overburden under Different Filling Quantities

Figure 3 shows the vertical stress distribution characteristics of the overburden under different filling quantities. It can be seen from Figure 3 that the stress balance of the surrounding rock of the working face was destroyed under the influence of mining. The stress was redistributed, a stress release zone was formed at the top and bottom of the working face, and a stress concentration zone was formed at the upper and lower ends of the working face, which were affected by the inclination of the coal seam. The stress release zone of the upper roof rock layer was larger than that of the lower roof rock layer. The stress release zone of the lower floor rock layer was larger than that of the upper part. The stress release zone of the slate layer at the bottom of the filling surface appeared in the lower part of the filling zone. The stress distribution characteristics of working faces were

the same when filling with different proportions of gangue. With the increase of filling quantities, the maximum stress values in the stress concentration zone were 28.7, 22.4, 22.1, 21.8, and 21.6 MPa, respectively. The maximum concentrated stress value decreased with the increase of filling amount, and the decrease of 1/5 of the maximum stress value was the most obvious compared with no filling. The vertical stress field of the overburden above the working face was asymmetric, and the shrinkage rate decreased with the increase of the filling amount. The vertical stress range of the overburden and the bottom plate in the filling zone increased significantly. It showed that the filling would bear and transmit the overburden stress. When the filling amount increased, the stress supported and transmitted by the filling would increase, so the filling had a better control effect on the overburden.

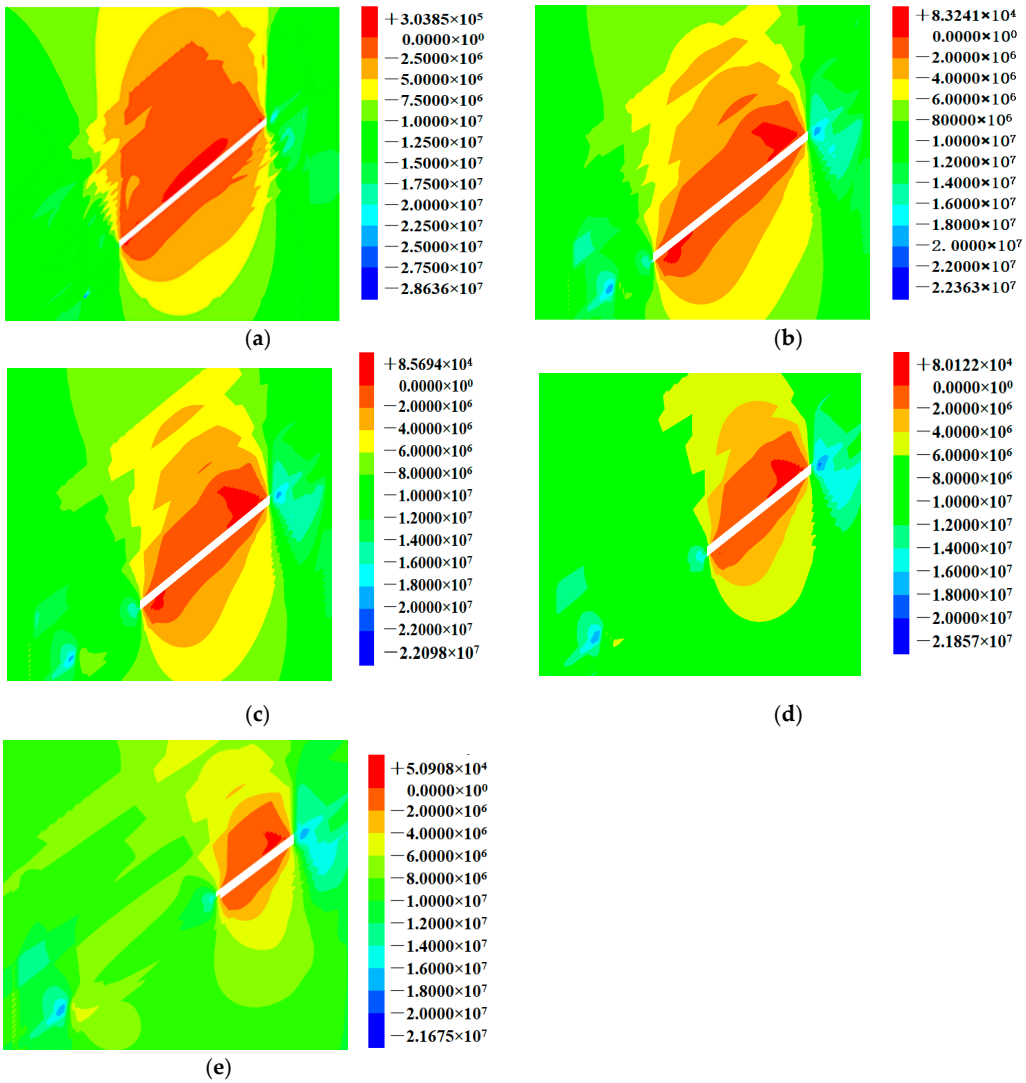

Figure 3. Vertical stress characteristics of overburden under different filling quantities. Different colors represent different vertical stress values as shown in the right legend. (**a**) No filling; (**b**) Filling 1/5; (**c**) Filling 1/3; (**d**) Filling 1/2; (**e**) Filling 2/3.

3.2. Vertical Displacement Distribution Characteristics of Overburden under Different Filling Quantities

Figure 4 shows the vertical displacement distribution characteristics of overburden under different filling quantities. It can be seen from Figure 4 that the displacement of the roof was the largest and the displacement of the floor was small during the SDCS gangue filling mining process. Due to the influence of coal seam inclination, the affected zone of vertical displacement of the roof moved to the upper part of the working face, and the affected zone

of displacement the floor moved to the lower part. With the different proportions of gangue filling in the working face, the vertical displacement of the roof and floor and the affected zone of the vertical displacement of the overburden were reduced to varying degrees.

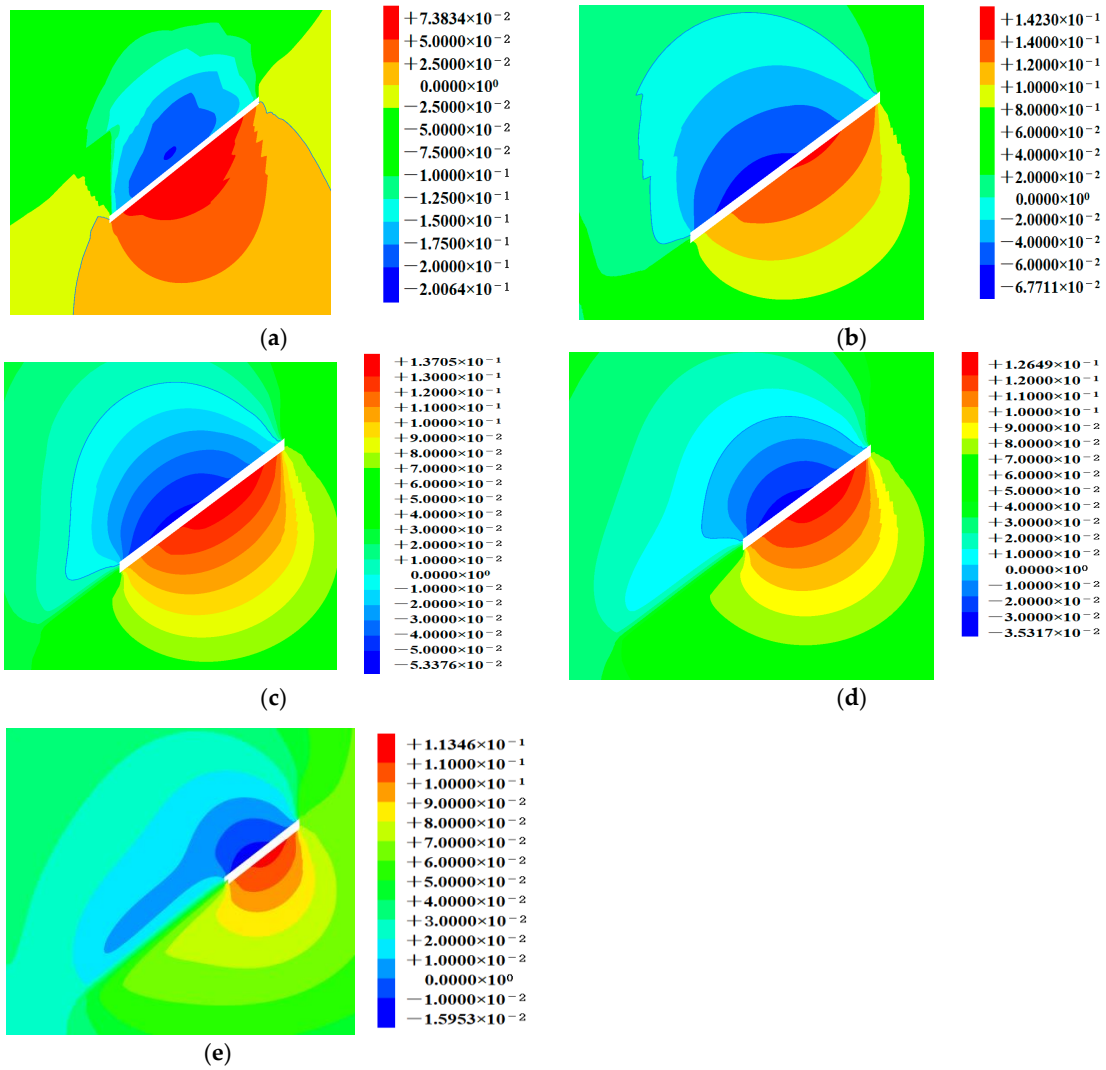

Figure 4. Vertical displacement distribution characteristics of overburden under different filling quantities. Different colors represent different vertical displacement values as shown in the right legend. (**a**) No filling; (**b**) Filling 1/5; (**c**) Filling 1/3; (**d**) Filling 1/2; (**e**) Filling 2/3.

The roof and overburden of the working face all showed downward displacement, and the maximum displacement of the vertical roof was 249 mm. After the working face was filled with gangue in different proportions, the vertical displacement of the overburden and the roof was effectively restrained. The range of the zero-displacement contour line of the roof in the unfilled zone decreased gradually, and the dip angle between the filled zone and the upper zero displacement contour line decreased with the increase of filling ratio. The vertical displacement of the lower overburden of the filling was smaller than that of the upper overburden, indicating that the upper end of the filling was greatly compressed by the concentrated stress. The vertical displacement of the overburden in the middle and lower part of the filling was the same, indicating that the filling was compressed and cooperated with the overburden to bear the pressure of it. The filling and the entire overburden were compressively deformed together to bear the pressure of the overburden. With the increase of the filling quantities, the influence height of the vertical displacement of the overburden decreased from 73 (filling 1/5) to 17.5 m

(filling 2/3). The effect range of the total vertical displacement was also small. With the filling ratio increases, the overburden migration was well-controlled.

3.3. Distribution Characteristics of the Overburden Plastic Zone under Different Filling Quantities

Figure 5 shows the distribution characteristics of the overburden plastic zone under different filling quantities. As shown in Figure 5, under the condition of no filling, the roof of the working face was mainly sheared, and both tensile and shear failure were shown in a small range of the floor. The range of the plastic zone and the overburden of the roof were much larger than the floor. The plastic zone of the roof and floor of the working face was asymmetrical under the influence of the inclination angle. The size of the lower plastic zone of the roof was larger than that of the upper zone, and the upper plastic zone of the floor was larger than that of the lower zone. Under the condition of local gangue filling, the roof rock of gangue filling zone was sheared. The upper roof rock of the unfilled zone was tensiled, and the lower roof rock in the unfilled zone and the floor rock in the working face were tensiled and sheared. When the filling ratio was 1/5 and 1/3, the plastic zone of the lower roof rock in the unfilled zone was larger than that of the upper zone, and the upper plastic zone of the working face was larger than that of the lower zone. When the filling ratio was 1/2 and 2/3, the range of the roof plastic zone in the unfilled zone was symmetrical along with the working face, and the upper floor plastic zone in the unfilled zone was still larger than that of the lower floor. Under the conditions of different filling quantities, the plastic zone of the roof in the working face was larger than that of the floor. The overall plastic zone decreased as the gangue filling ratio increased, and the plastic zone of the roof and floor in the filling zone tended to be stable.

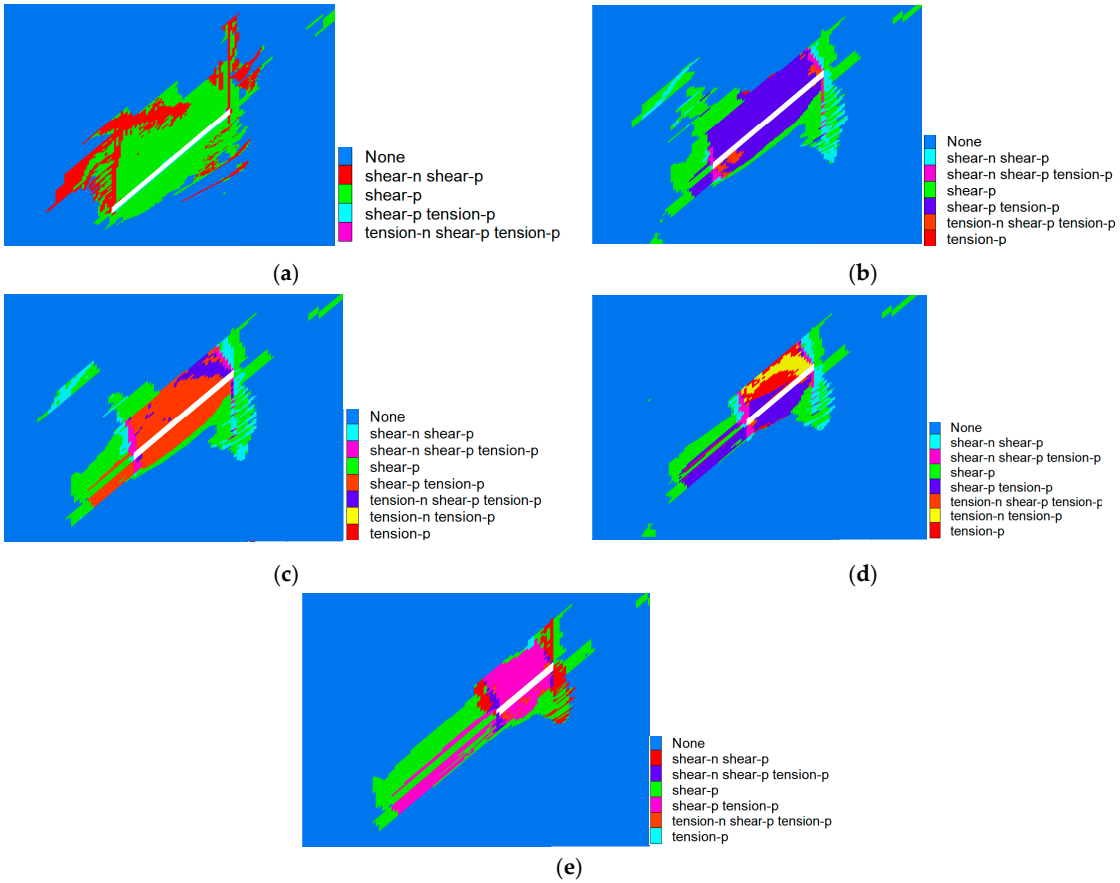

Figure 5. Distribution characteristics and tendency of the overburden plastic zone under different filling quantities. Different colors represent different plastic zone as shown in the right legend. (**a**) No filling; (**b**) Filling 1/5; (**c**) Filling 1/3; (**d**) Filling 1/2; (**e**) Filling 2/3.

3.4. Overburden Evolution Law

3.4.1. Overburden Collapse Form

Figure 6 shows the overburden collapsed form during local gangue filling mining. As shown in Figure 6, in the early stage of model mining, the immediate roof of the goaf behind the working face collapsed first, and the direct low-level roof adjacent to the working face also collapsed. When the working face was advanced to 80 m, the overburden collapse height had developed to the low rock layer above the main roof. The roof at the lower end of the gangue filling zone did not collapse, but the immediate roof collapsed in the form of interval collapse along the strike. When the working face was advanced to 120 m, the overburden collapse height developed upward, the effective support zone of the gangue filling decreased, and the roof collapse range at the lower end of the gangue filling zone got larger. When the working face was advanced to 160 m, the mining of the model working face was completed, and the collapsed height was developed from the main roof to three rock layers. The roof collapse range at the lower end of the gangue filling zone of the working face was further expanded, but no roof collapse was found on the excavation side. The position of the arch shell vault appeared in the middle and lower part of the unfilled zone in the working face. After the model mining was completed, the stress release zone of the roof was mainly concentrated in the upper roof and the floor stratum at the lower part in the working face. The stress release zone of the roof rock stratum was larger than that of the floor stratum. In the strike direction, the stress release in the middle was the most adequate.

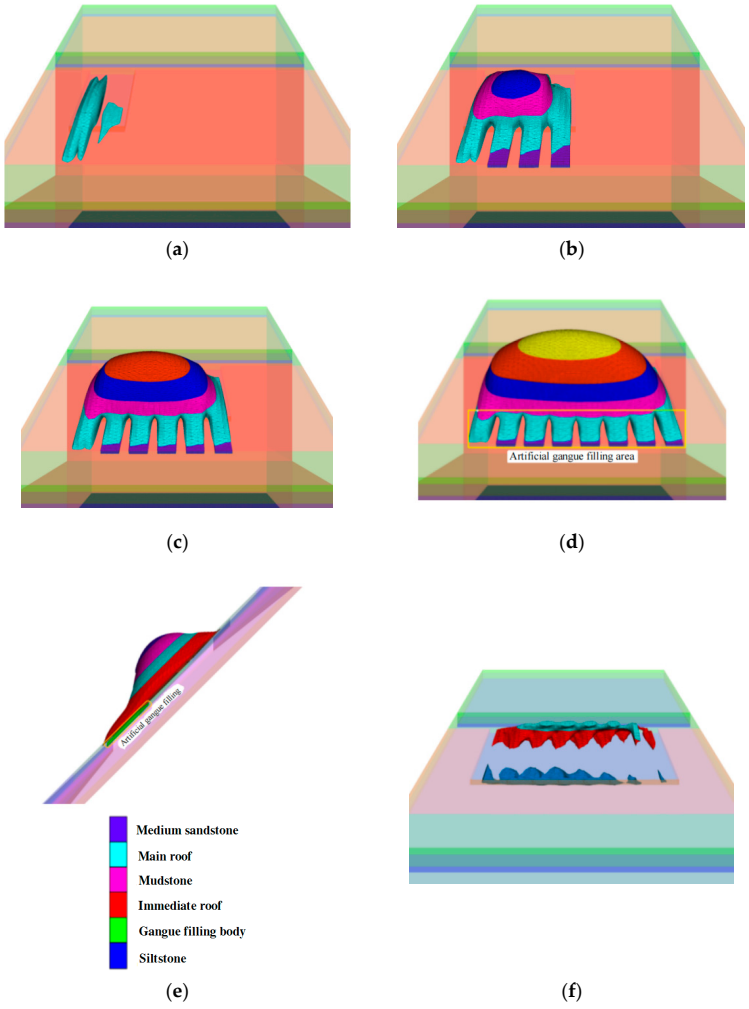

Figure 6. Overburden collapse form of local filling mining. Different colors represent different layers. (**a**) 40 m; (**b**) 80 m; (**c**) 120 m; (**d**) 160 m; (**e**) Inclined overburden collapse form; (**f**) Overburden stress release zone.

It can be seen from Figure 7a that the immediate roof at the lower part of the gangue filling zone was not in contact with the gangue. The immediate roof turned clockwise, and the gangue at the upper end of the filling was squeezed and deformed by the roof, indicating that the filling was stress-concentrated. Then, a measurement line was arranged advanced along the working face in the gangue filling. Then, a survey line was arranged advanced along the working face in the gangue filling. The maximum displacement of the upper end of the filling was obtained from the survey line. The plastic failure occurred at the upper end of the filling. The vertical stress value decreased suddenly, which was consistent with the distribution characteristics of the filling bearing pressure in the physical similarity simulation experiment.

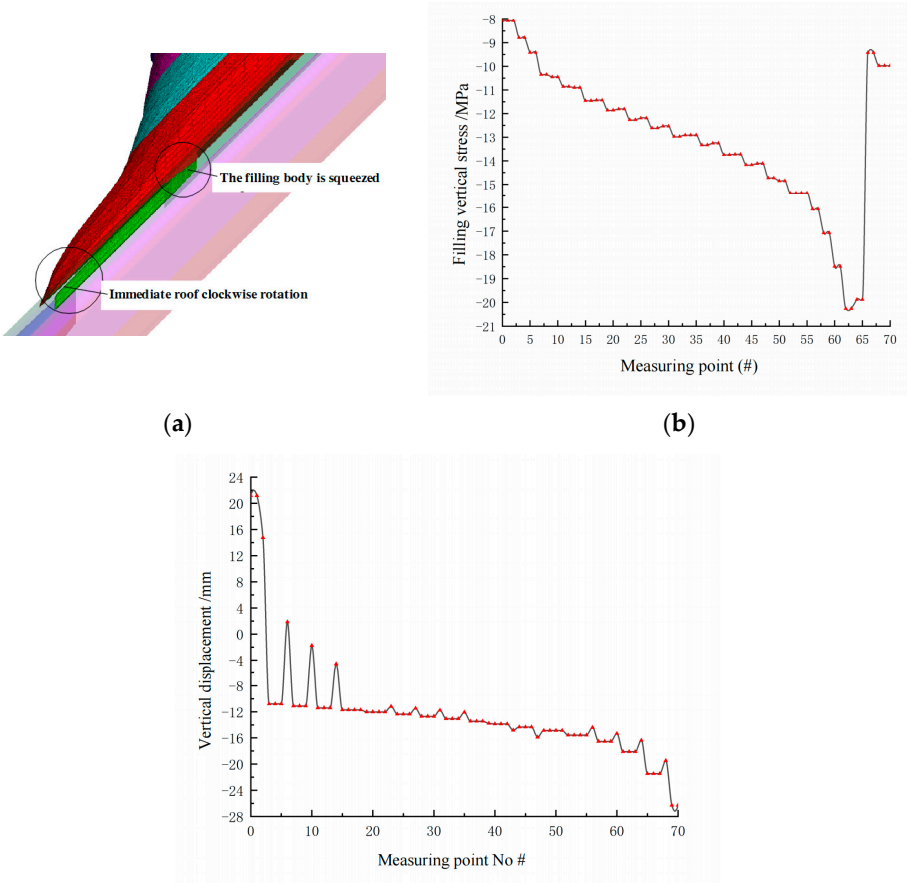

Figure 7. Bearing pressure distribution characteristics of filling. (**a**) Abutment pressure of filling, shows the immediate roof at the lower part of the gangue filling zone turned clockwise; (**b**) Vertical stress of the filling, and (**c**) Vertical displacement of filling, show the vertical stress and displacement of the filling, respectively.

3.4.2. Main Roof Displacement and Stress Evolution Characteristics

The evolution characteristics of main roof displacement are shown in Figure 8. As shown in Figure 8, on the condition of 1/3 filling, as the working face was advanced to 40 m, the main roof of the goaf moved upward, and there was an upward displacement behind the excavation and in front of the coal wall. The rear displacement behind the excavation was 29 mm, and the displacement in front of the coal wall was 50 mm. On the condition of no filling, the upward displacement behind the excavation was 25 mm, and no obvious displacement was found in the main roof of the untapped coal seam behind the coal wall.

With the working face advanced, the deformation degree of the main roof increased gradually under the two working conditions, and the roof of the undrawn coal seam in front of the coal wall showed downward vertical displacement with different degrees.

The maximum deformation of the unfilled roof was four times that of the filling, and the maximum deformation of the displacement in both working conditions occurred in the middle of the working face trend. Filling mining would move the main roof at both ends of the working face upward along the strike. After the first filling, the displacement of the roof at both ends of the working face along the strike had reached the maximum upward displacement. This was due to the main roof of the working face being regarded as a simple beam structure. During the working face advance along the strike, the middle part of the main roof was broken, and the two ends of the working face were deflected upward under the support of the coal pillar, so the two ends would deflect upward displacement [32–34].

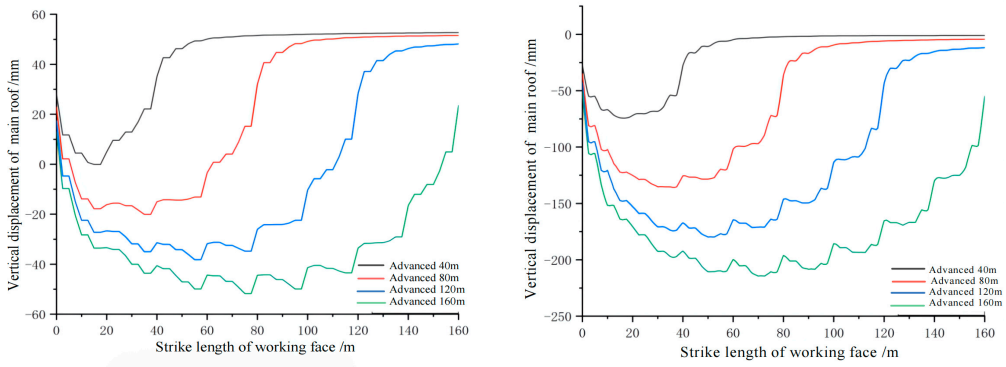

Figure 8. The evolution characteristics of main roof displacement. This figure shows the relationship between vertical displacement of main roof and the advanced length of the working face in filling 1/3 and no filling. (**a**) Filling 1/3; (**b**) No filling.

The evolution characteristics of the main roof stress are shown in Figure 9. As shown in Figure 9, the vertical stress of the main roof in front of the coal wall was greater than that behind the excavation hole. Under the two working conditions, the stress release degree of the main roof without filling was greater than that of the filling mining. Under the filling condition, the stress of the roof behind the excavation hole was maintained as 4–5 MPa. Under the condition of no filling, the stress of the roof behind the excavation hole was 10.3 Mpa as the working face was advanced to 40 m and 11.6 MPa as the working face was advanced to 80 m. When the working face was advanced to 120 m, the stress decreased suddenly to 4.2 MPa and kept at 4–5 MPa, indicating that the roof was collapsed. During the whole advancing process, the peak stress of the filling mining was smaller than that of the non-fill, and no large-scale roof pressure release was found.

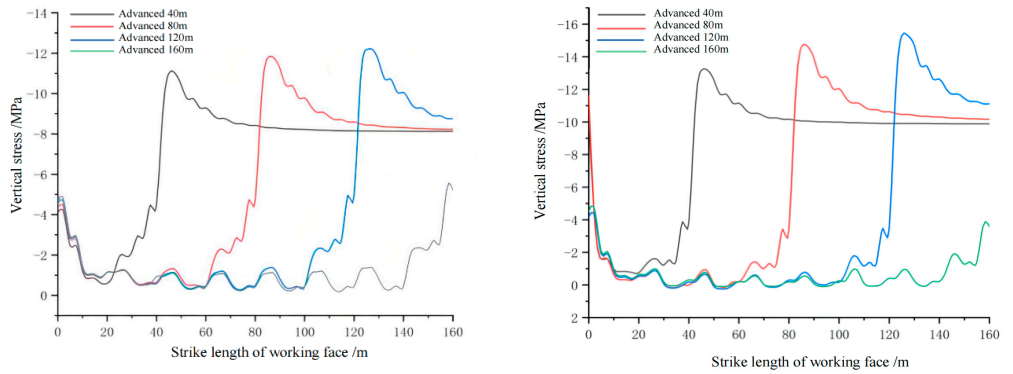

Figure 9. Evolution characteristics of main roof stress. This figure shows the relationship between vertical stress and the advanced length of the working face in filling 1/3 and no filling. (**a**) Filling 1/3; (**b**) No filling.

4. Establishment and Analysis of Physical Similarity Simulation Experiment

4.1. Establishment of Physical Model

Taking the working face 3221 of Lvshuidong Coal Mine as the engineering background, the experiment was conducted on a test frame with a variable angle. The model size was 2150 mm× 200 mm× 1800 mm in length × width × height, respectively. According to the in situ engineering and the model size, the geometric similarity ratio was set as 1:50. According to the similarity principle and dimensional analysis, the unit weight similarity constant was set as 1.6, the stress similarity constant was set as 80, and the time similarity constant was set as $\sqrt{50}$. The aggregates were river sand and fly ash, the bonding materials were gypsum and white powder, and the layered materials were mica powder [35,36]. Table 2 shows the proportion of similar materials.

Table 2. The proportion of similar materials.

Name	Coal Rock Name	Coal Rock Thickness (m)	Model Thickness (cm)	Proportioning (Sand, Gypsum, White)
Main roof	Marl	7.20	14.4	755
Immediate roof	Sandy mudstone	8.60	17.2	737
Coal	Coal	3.20	6.4	21:1:2:21 (flying ash)
Immediate floor	Mudstone	5.30	10.6	737
Main floor	Sandstone	4.40	8.8	746

The physical similarity simulation experiment adopted the two-dimensional inclined model frame with variable angle, and the wireless pressure sensor was buried in the coal seam during the laying process of the experimental model. The measuring points were arranged on the surface of the model frame, and a Pentax-400 nx optical total station was used to monitor the movement of the overburden when the frame was moved. The hydraulic support in the actual working face is simulated by a simple support. Throughout the experiment, a high-speed camera was used to record the overburden collapse form and the entire collapse process. The monitoring equipment is shown in Figure 10.

When the physical similarity model was laid, a pressure sensor was buried in the coal seam to monitor the pressure on the floor. Eight survey lines were arranged in the coal seam, among which the *a* and *b* survey lines were arranged on the immediate roof and the main roof, respectively. The distance between the measuring points and measuring lines was 10 cm, and the width of the working face was 160 cm (corresponding to the actual engineering, 80 m). During the test, a support was used to replace the filling, and a certain initial force was given to support the roof and the overburden. After the whole working face was mined, a total of 38 simple supports were installed as shown in Figure 11. After the support installation of the working face was completed, all supports on the working face were withdrawn quickly to simulate the removal of the frame on the non-fill working face.

The support of the working face was installed with 1/3 filling and simulated as shown in Figure 11. The whole filling width was 1–13#, and the total length of the support was 54 cm (corresponding to the in situ engineering, 27 m). The retractable support replaced the gangue, and the working face was filled with the support moving with the working face. The working resistance of the support was reduced to passive support for the roof to achieve the purpose of manual loading gangue. When the partial filling of the working face was completed, the remaining stents were removed quickly.

(**a**) (**b**)

(**c**)

Figure 10. Monitoring equipment. This figure shows the optical total station, the simple support, and the high-speed camera, respectively. The equipment was used in the observation of the physical model test. (**a**) Optical total station; (**b**) Simple support; (**c**) High-speed camera.

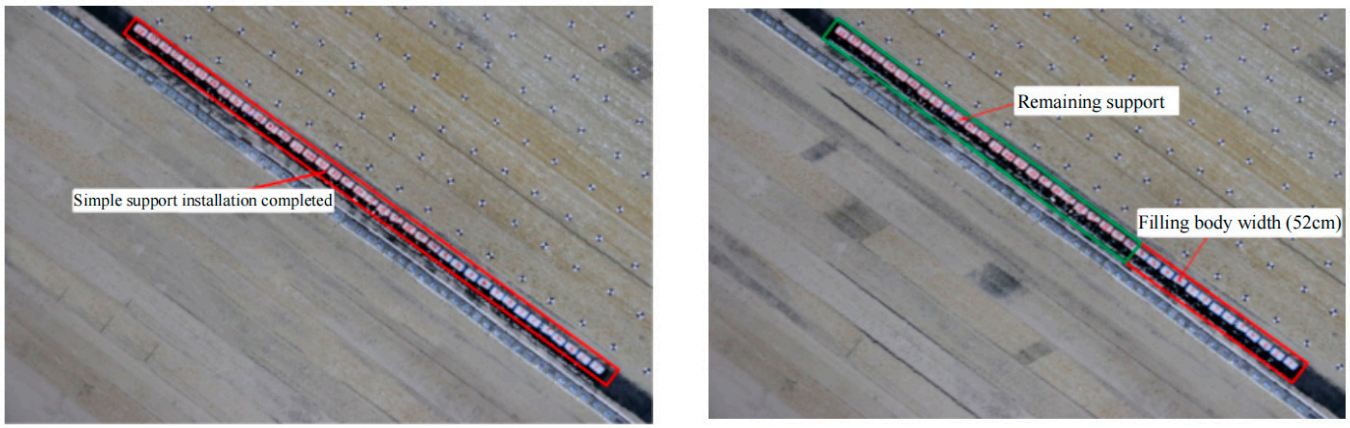

(**a**) (**b**)

Figure 11. Model of the physical simulation experiment. (**a**) No filling; (**b**) Filling 1/3. The red mark in (**a**) shows the installation completed of simple support in no filling, the red mark and green mark in (**b**) show the filling width (52 cm) and remaining support, respectively.

4.2. Analysis of the Physical Simulation Results

4.2.1. Law of the Overburden Failure

Figure 12 shows the overburden collapse morphology at no filling and 1/3 filling. It can be seen from the figure that the stability of the support system was destroyed after the working face frame was removed. The pressure on the overburden of the working face changed from the overall compression to tensile and shear stress before the frame was removed. The tensile properties of the overburden were weak and more easily damaged. The immediate roof slid down to the lower part of the working face under the action of the gravity, and the broken roof was piled up and compacted at the lower part of the working face to support the lower overburden of the working face. The collapsed strata slid down and squeezed each other under the action of its own weight, which led to the closure of the cracks between the collapsed rocks at the lower part of the working face, so that the overburden at the upper part of the working face collapsed more fully. As the goaf was not filled, the lower collapse angle was 53°, the upper span angle was 49°, the maximum collapse height was 66.7 cm, and the roof suspension beam length was 55.5 cm. When filling 1/3, the collapse angle of lower overburden was 55°, the upper span angle was 50°, the maximum collapse height was 42 cm, and the roof suspension beam was 33.1 cm. Compared with that of the non-fill overburden, the collapsed height of the 1/3 filled overburden was reduced by 37%, the failure mode of the overburden was asymmetric, the overall collapse range was reduced, and the overburden collapsed only in the unfilled zone. A small separation of the overburden occurred in the filling zone, indicating that the movement and failure of the overburden could be controlled effectively by the filling mining.

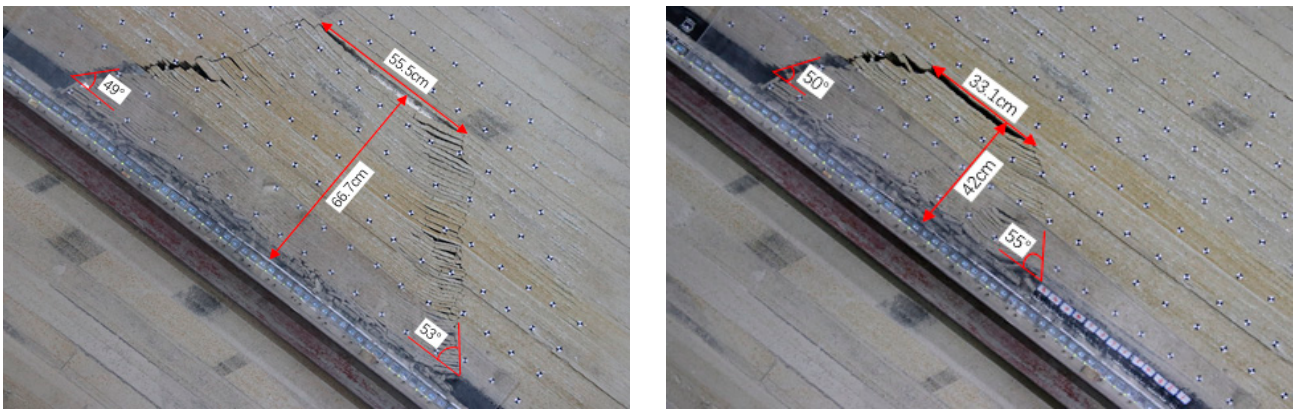

(**a**) (**b**)

Figure 12. Collapse form of the overburden. This figure shows the height, inclination angle, and the top length of the collapse in no filling and filling 1/3, respectively. (**a**) No filling; (**b**) Filling 1/3.

4.2.2. Vertical Displacement of the Overburden

Figure 13 shows the vertical displacement variation of the immediate roof and main roof, respectively. According to comparative analysis, the maximum vertical displacement of the unfilled immediate roof was 69.4 mm. The immediate roof was 62.3 mm at filling 1/3, which was 7.1 mm less than that of the unfilled mining. The maximum vertical displacement of the main roof was 41.8 mm under no filling condition and 34.7 mm under 1/3 filling condition. The vertical displacement of the main roof was also reduced by 7.1 mm as compared with that of no filling. The maximum vertical displacement of both was in the upper part of the working face. The variation trend of the vertical displacement of the roof was similar. The top to bottom distribution of the vertical displacement of the working face was that the upper part of it was the largest, the middle part of it was the second, and the lower part of it was the smallest. The vertical displacement of the direct and main roof in filling mining was less than that in non-fill mining. The overall downward movement of the overburden in filling mining was small. The vertical displacement of the

immediate roof and the main roof above the filling zone varied the same, and the vertical displacement was almost zero. It showed that the filling had a good inhibitory effect on the movement of the overburden.

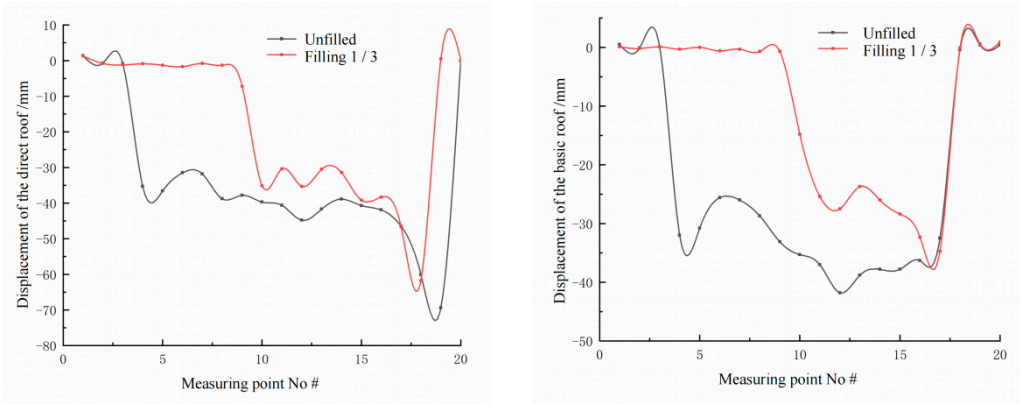

(**a**) (**b**)

Figure 13. Vertical displacement of the roof. This figure shows the displacement of the main roof in different measuring points of the immediate roof and main roof. (**a**) Immediate roof; (**b**) Main roof.

4.2.3. Bearing Pressure Distribution Characteristics of the Overburden

After the physical similarity model was built, data of the pressure sensor in the coal seam floor was collected, and the stress curve in the original rock was obtained after processing, analysis, and fitting. The original rock stress in the coal seam was approximately linear from bottom to top.

Figure 14 shows the relationship between the support of the working face and the support pressure of the upper and lower coal pillars after the support installation in the whole working face during non-fill mining. It can be seen from Figure 14 that when the working face was supported, the average support pressure and the maximum support pressure of the coal pillar at the lower end of the working face were greater than those at the upper end of the working face. The maximum bearing pressures of the upper and lower coal pillars were 7.2 and 9.45 MPa, respectively, while the bearing pressure in the middle of the working face was greater than the original rock stress. After the coal seam was excavated, the overburden stress was released fully due to the disturbance of the surrounding rock until the surrounding rock pressure was rebalanced.

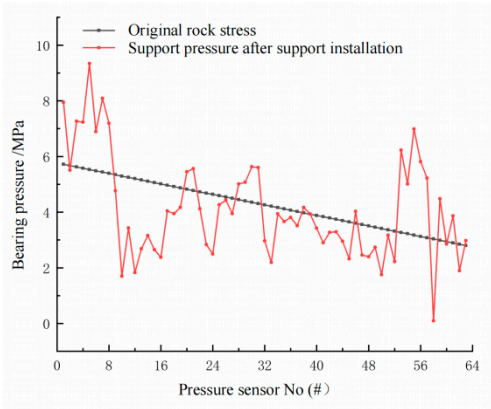

Figure 14. Bearing pressure of the floor after the support installed in the working face.

Figure 15 shows the support pressure curves during unfilled and filling 1/3. According to comparative analysis, it could be seen that the overburden was broken and collapsed three times after the support was withdrawn from the working face, which formed stress concentration in the upper and lower coal pillars. At no filling, the average stresses of the

upper and lower coal pillars were 18 and 8.5 MPa, respectively. The stress concentration of the upper coal pillar was much larger than that of the lower coal pillar. When filling 1/3, the overburden was broken and collapsed once, and the stress concentrated in the upper and lower coal pillars were 10 and 11 MPa, respectively. Under the action of filling, the overburden stress was transmitted downward, which resulted in a slight difference between two of them. Due to the influence of the working face excavation on the filling and the coal pillar, a stress mutation occurred at the junction of the filling and the lower coal pillar. The supporting pressure curve of the whole filling increased approximately linearly, with a minimum value of 2.6 MPa and a maximum value of 8.1 MPa. The average value was 5 MPa, which was much larger than the support pressure of the unfilled floor. When filling 1/3, the support pressure of the upper coal pillar was also 7 MPa lower than that of no filling, indicating that the influence of stress concentration could be transferred and reduced by filling mining played a certain role in the overburden support.

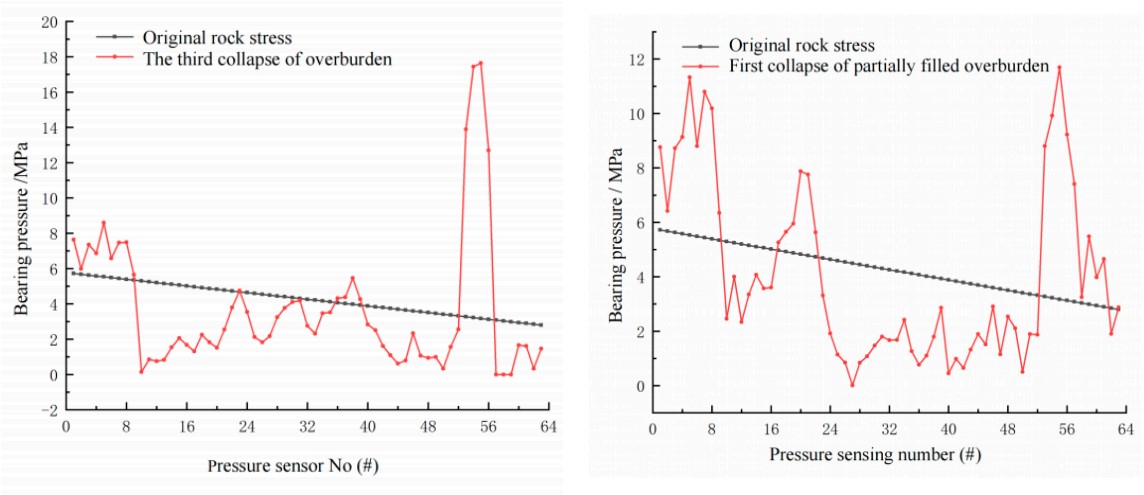

(**a**) (**b**)

Figure 15. Bearing pressure of the floor. This figure shows the bearing pressure of the floor in no filling and filling 1/3. (**a**) No filling; (**b**) Filling 1/3.

By analyzing the pressure distribution characteristics on the support of the filling, as shown in Figure 16, it could be concluded that the support stress of the filling body increased gradually from the lower end of the working face to the upper end. The stress concentration occurred when the filling approached the upper end. The correlated software analysis performed linear fitting on the support pressure of the filling. The linear equation of the support pressure of the filling was obtained as follows, $y = 1.28 + 0.14x$.

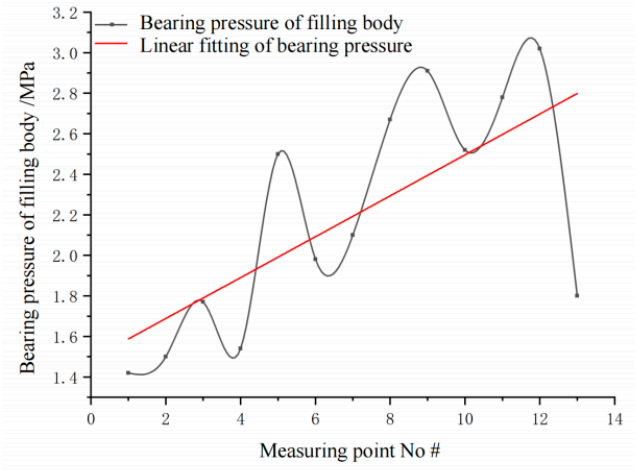

Figure 16. Pressure distribution characteristics on the support of the filling.

5. Conclusions

As the filling ratio increased, the maximum stress in the stress concentration zone decreased. Compared with no filling, the decrease of the maximum stress decrease was the most obvious at filling 1/5. The vertical stress field of the overburden above the working face was asymmetrically distributed, the shrinkage rate decreased as the filling quantities increased, and the vertical stress range of roof and floor in the filling zone increased significantly.

With the increase of filling ratio, the affected zone of vertical displacement of roof, floor, and overburden reduced to varying degrees. The contour line range of zero displacement in unfilled zone of the roof decreased gradually. As the filling ratio increased, the inclination angle between the filling zone and the upper zero displacement contour line decreased. The movement of the overburden was well-controlled as the proportion of the filling increased.

(1) As the filling ratio increased, the range of the overall plastic zone was decreased. The range of the roof plastic zone in the unfilled zone was symmetrical along the working face, but the plastic zone of the upper floor in the unfilled zone was still larger than that in the lower floor.
(2) To a certain extent, this paper revealed the influence of the filling scale on the mechanical behavior of the roof in the local filling mining of steeply dipping coal seams. The filling in the experiment was assumed to be an elastic foundation, but the actual situation may be more complicated. However, the relevant experimental research and field monitoring analysis on the three-dimensional filling characteristics of gangue were lacking at present, which needs to be supplemented in follow-up research.

Author Contributions: Conceptualization, S.W. and W.L.; supervision, W.Z.; funding acquisition, methodology, W.L. and S.W.; numerical calculation, K.G.; data curation, J.F.; writing—original draft preparation, W.L. and K.G.; physical similarity simulation experiment, A.L. and K.Z. All authors have read and agreed to the published version of the manuscript.

Funding: This research was funded by the National Natural Science Foundation of China (No. 51974226, 52174127), the Research Fund of Shaanxi Key Laboratory of Coal Mine Water Disaster Prevention and Control Technology (No. 2020SKMS02), and the Research Fund of Henan Key Laboratory for Green and Efficient Mining & Comprehensive Utilization of Mineral Resources (Henan Polytechnic University, No. KCF202001).

Data Availability Statement: Not applicable.

Acknowledgments: The authors would like to extend their sincere appreciation to the Sichuan Coal Industry Group Co., Ltd. for data collection.

Conflicts of Interest: The authors declare no conflict of interest.

References

1. Wu, Y.P.; Liu, K.Z.; Yun, D.F.; Xie, P.S.; Wang, H.W. Research progress of safe and efficient mining technology in steep seam. *J. China Coal. Soc.* **2014**, *39*, 1611–1618.
2. Wu, Y.P.; Yun, D.F.; Xie, P.S. *Theory and Technology of Longwall Fully Mechanized Mining in Large Dip Seam*; Science Press: Beijing, China, 2017.
3. Xie, P.S.; Wu, Y.P.; Luo, S.H.; Wang, H.W.; Lang, D. Evolution and stability analysis of inclined bench structure in large dip and high mining height stope. *China J. Rock Mech. Eng.* **2018**, *35*, 953–959.
4. Lv, W.Y.; Wu, Y.P.; Liu, M.; Yin, J.H. Migration law of the roof of a composited backfilling longwall face in a steeply dipping coal seam. *Minerals* **2019**, *9*, 188. [CrossRef]
5. Zhang, D.S.; Wu, X.; Zhang, W.; Fan, G.W. Stability analysis of support in special mining period of large dip face. *J. Min. Saf. Eng.* **2013**, *30*, 331–336.
6. Yin, G.Z.; Li, X.S.; Guo, W.B. Pseudo model test and field measurement of photoelastic modulus of surrounding rock pressure distribution law of large dip coal seam working face. *China J. Rock Mech. Eng.* **2010**, *29*, 3336–3343.
7. Wang, J.A.; Jiao, J.L. Criteria of support stability in mining steeply inclined thick coal seam. *Int. J. Rock Mech. Min.* **2016**, *82*, 22–35. [CrossRef]
8. Cao, S.G.; Xu, J.; Lei, C.G.; Peng, Y.; Liu, H.L. Adaptability analysis of support in steeply inclined fully mechanized mining face under complex conditions. *J. China Coal. Soc.* **2010**, *35*, 1599–1603.

9. Kostecki, T.; Spearing, A.J.S. Influence of backfill on coal pillar strength and floor bearing capacity in weak floor conditions in the Illinois Basin. *Int. J. Rock Mech. Min.* **2015**, *76*, 55–67. [CrossRef]
10. Qiu, H.F.; Zhang, F.S.; Liu, L. Experimental study on acoustic emission characteristics of cemented rock-tailings backfill. *Constr. Build. Mater.* **2022**, *315*, 125278. [CrossRef]
11. Lu, B.; Li, Y.L.; Fang, S.Z.; Lin, H.; Zhu, Y. Cemented backfilling mining technology for gently inclined coal seams using a continuous mining and continuous backfilling method. *Shock Vib.* **2021**, *2021*, 6652309. [CrossRef]
12. Panchal, S.; Deb, D.; Sreenivas, T. Mill tailings based composites as paste backfill in mines of U-bearing dolomitic limestone ore. *J. Rock Mech. Geotech. Eng.* **2018**, *10*, 310–322. [CrossRef]
13. Li, S.; Zhao, Z.M.; Yu, H.X.; Wang, X.M. The recent progress china has made in the backfill mining method, part II: The composition and typical examples of backfill systems. *Minerals* **2021**, *11*, 1362. [CrossRef]
14. Yilmaz, E.; Belem, T.; Benzaazoua, M. Effects of curing and stress conditions on hydromechanical, geotechnical and geochemical properties of cemented paste backfill. *Eng. Geol.* **2014**, *168*, 23–37. [CrossRef]
15. Al Heib, M.M.; Didier, C.; Masrouri, F. Improving short- and long-term stability of underground gypsum mine using partial and total backfill. *Rock Mech. Rock Eng.* **2010**, *43*, 447–461. [CrossRef]
16. Cheng, Q.Q.; Guo, Y.B.; Dong, C.W.; Xu, J.F.; Lai, W.A.; Du, B. Mechanical properties of clay based cemented paste backfill for coal recovery from deep mines. *Energies* **2021**, *14*, 5764. [CrossRef]
17. Khaldoun, A.; Ouadif, L.; Baba, K.; Bahi, L. Valorization of mining waste and tailings through paste backfilling solution, Imiter operation, Morocco. *Int. J. Min. Sci. Technol.* **2016**, *26*, 146–151. [CrossRef]
18. Zhao, Y.; Taheri, A.; Karakus, M.; Deng, A.; Guo, L. The effect of curing under applied stress on the mechanical performance of cement paste backfifill. *Minerals* **2021**, *11*, 1107. [CrossRef]
19. Xie, P.S.; Wu, Y.P. Stability analysis of inclined masonry structure and support in longwall stope of large dip seam. *J. China Coal. Soc.* **2012**, *37*, 1275–1280.
20. Yao, Q.; Feng, T.; Liao, Z. Instability mechanism and reasonable size of sharply inclined segmented filling column. *J. Min. Saf. Eng.* **2018**, *35*, 49–57.
21. Guo, J.Z.; Meng, X.R.; Gao, Z.N. Numerical simulation of ground pressure law in steeply dipping coal seam. *Coal. Min.* **2011**, *16*, 97–99.
22. Xiao, J.P.; Yang, K.; Liu, S.; Zhou, B. Study on overburden breaking mechanism in mining of steeply dipping coal seam. *J. Saf. Sci. Tech.* **2019**, *15*, 75–80.
23. Wang, H.W.; Wu, Y.P.; Xie, P.S. Coal rib stability effect of mining-thickness with large mining height of working face in steeply inclined seams. *J. Min. Saf. Eng.* **2018**, *35*, 64–70. [CrossRef]
24. Dudek, M.; Tajduś, K. FEM for prediction of surface deformations induced by flooding of steeply inclined mining seams. *Geomech. Energy Environ.* **2021**, *28*, 100254. [CrossRef]
25. Ross, C.; Conover, D.; Baine, J. Highwall mining of thick, steeply dipping coal–a case study in geotechnical design and recovery optimization. *Int. J. Min. Sci. Technol.* **2019**, *29*, 777–780. [CrossRef]
26. Zhao, X.D.; Jiang, J.; Lan, B.C. An integrated method to calculate the spatial distribution of overburden strata failure in longwall mines by coupling GIS and FLAC3d. *Int. J. Min. Sci. Technol.* **2015**, *3*, 369–373. [CrossRef]
27. Kong, P.; Jiang, L.S.; Shu, J.M.; Wang, L. Mining stress distribution and fault-slip behavior: A case study of fault-influenced longwall coal mining. *Energies* **2019**, *12*, 2494. [CrossRef]
28. Zhang, J.X.; Li, B.Y.; Zhou, N.; Zhang, Q. Application of solid backfilling to reduce hard-roof caving and longwall coal face burst potential. Int. *J. Rock Mech. Min.* **2016**, *88*, 197–205.
29. Maleska, T.; Beben, D.; Nowacka, J. Seismic vulnerability of a soil-steel composite tunnel—Norway Tolpinrud Railway Tunnel Case Study. *Tunn. Undergr. Space Technol.* **2021**, *110*, 103808. [CrossRef]
30. Ramada, S.H.; Naggar, M.H.E. Class-A prediction of three-sided reinforced concrete culverts and numerical investigation of the supporting strip footing geometry effect. *Struct. Infrastruct. E* **2021**, *14*, 3409. [CrossRef]
31. Zhou, H.Z.; Xu, H.J.; Yang, P.B.; Zheng, G.; Liu, X.N.; Zhang, W.B.; Zhao, J.P.; Yu, X.X. Centrifuge and numerical modelling of the seismic response of tunnels in two-layered soils. *Tunn. Undergr. Space Technol.* **2021**, *113*, 103980. [CrossRef]
32. Wu, Y.P. *Basic Research on Dynamic Control of "R-S-F" System in Large Dip Seam Mining*; Shaanxi Science and Technology Press: Xi'an, China, 2003.
33. Xie, S.R.; Zhang, G.C.; Zhang, S.B.; He, F.L.; Xiao, D.C. Study on support surrounding rock stability control of large dip Island fully mechanized mining face. *J. Min. Saf. Eng.* **2013**, *30*, 343–347.
34. Yang, K.; Chi, X.L.; Liu, S. Instability mechanism and control of hydraulic support in fully mechanized mining face with large dip seam. *J. China Coal. Soc.* **2018**, *43*, 1821–1828.
35. Dai, H.X.; Yi, S.H.; Guo, J.T.; Yan, Y.T.; Liu, A.J. Prediction method of surface movement in horizontal layered mining of extra thick and steep coal seam. *J. China Coal. Soc.* **2013**, *38*, 1305–1311.
36. Hu, B.S.; Wu, Y.P.; Wang, H.W.; Tang, Y.P.; Wang, C.R. Risk mitigation for rockfall hazards in steeply dipping coal seam: A case study in Xinjiang, northwestern China. *Geomat. Nat. Hazards Risk* **2021**, *12*, 988–1014. [CrossRef]